Contribution from the Department of Chemistry,
University of Pittsburgh, Pittsburgh, Pennsylvania 15260

Autoxidation Mechanism of $Fe_2(ttha)^{2-}$ and Studies of $[Me_2Dabco][Fe_2O(ttha)]\cdot 6H_2O$

Rex E. Shepherd,* Terry K. Myser, and Michael G. Elliott

Received August 7, 1987

The reaction of O_2 and $Fe_2(ttha)^{2-}$ ($ttha^{6-}$ = triethylenetetraminehexaacetate) was shown to obey a rate law $d[Fe_2O(ttha)^{2-}]/dt = \{[K_{O_2}k_1k_2[H^+]/(k_{-1} + k_2[H^+])] + k_0\}[Fe_2(ttha)^{2-}][O_2]$ with $K_{O_2}k_1 = 3.32 \times 10^2\ M^{-1}\ s^{-1}$, $k_2/k_{-1} = 3.01 \times 10^6\ M^{-1}$, and $k_0 = 63\ M^{-1}\ s^{-1}$. The mechanism of oxidation is discussed in terms of the equilibrium binding of O_2 forming an $[(Fe^{III}O_2^-)ttha(Fe^{II})]$ intermediate in an open-chain configuration. For the proton-dependent pathway, this step is followed by ring closure, forming a peroxo intermediate that is reduced rapidly after protonation. No free O_2^- or O_2^{2-} is detected by competitive trapping experiments with superoxide dismutase or catalase enzymes. The presence of inner-sphere O_2^-, bound in the intermediate, is implicated by spin-trapping experiments using DMPO (5,5-dimethyl-1-pyrroline *N*-oxide) as the radical trap. When $Fe_2(ttha)^{2-}$ is oxidized by H_2O_2, the HODMPO• adduct is readily detected by its characteristic four-line 1:2:2:1 pattern ($a_N = a_H = 15.0$ G) in its ESR spectrum. The bound O_2^- intermediate in the $Fe_2(ttha)^{2-}$ autoxidation scheme will extract an H atom from C_2H_5OH in its solvent cage; the DMPO adduct of CH_3CHOH is trapped, giving a pattern of six equal lines ($a_N = 16.0$ G, $a_H = 22.8$ G). A maximum of 6% of the pathway results in a carbon-centered radical; the remainder of the reduction events produce $Fe_2O(ttha)^{2-}$ by rapid reduction of the $[Fe^{III}_2(O_2^{2-})(ttha)]^{2-}$ intermediate. The $Fe_2O(ttha)^{2-}$ ion was precipitated as its Me_2Dabco^{2+} salt. This compound was shown to have ferric ions in an $^6A_1$ state; the Mössbauer spectrum yielded 0.63 mm/s for the isomer shift and 1.56 mm/s for the quadrupole splitting parameter vs sodium nitroprusside. The solid exhibited an Fe–O–Fe asymmetric stretch at 833 cm^{-1} for ^{16}O and 846 cm^{-1} for the ^{18}O-labeled complex. The UV–visible spectrum is very similar to that of the $Fe_2(hedta)_2^{2-}$ complex. The absorption maximum occurs at 470 nm (ϵ/Fe = 80 $M^{-1}\ cm^{-1}$) compared to the same $\{^6A \rightarrow [^4A_1, {}^4E]\ (^4G)\}$ transition of $Fe_2O(hedta)_2^{2-}$ at λ_{max} = 475 nm (ϵ = 180 $M^{-1}\ cm^{-1}$).

Introduction

Triethylenetetraminehexaacetate, $ttha^{6-}$, forms binuclear complexes that may exist either in an extended-chain geometry (**1A**) or in a bridged form (**1B**). The two structural forms may have

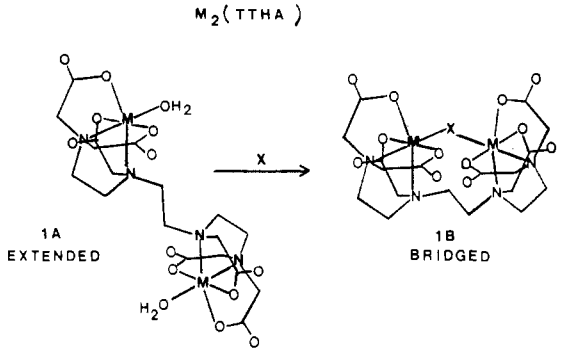

greatly different chemical reactivities. For example, the V(III) binuclear complex exists in the extended form at pH ~3 and reacts slowly with O_2, while the oxo-bridged $V_2O(ttha)^{2-}$ complex (pH ~7) reacts rapidly with O_2 to form a $[V^{III}V^{IV}O_2^-]$ intermediate.[1] The V(IV) binuclear complex crystallizes in the extended form,[2] but its solution structure is bridged, as evidenced by ESR.[1,3] Similarities between $V_2O(ttha)^{2-}$ and $Fe_2O(hedta)_2^{2-}$ led us to conduct parallel experiments using Fe(II) and Fe(III) binuclear complexes of $ttha^{6-}$. Binuclear Fe(II) and Fe(III) complexes of $ttha^{6-}$ were characterized in titrimetric studies by Schroder,[4] Harju,[5,6] and Martell and Bohigan.[7] The $Fe^{II}_2(ttha)^{2-}$ species exists in the extended form[4] while the Fe(III) binuclear complex is bridged.[4-7] The formulation $Fe_2(OH)_2(ttha)^{2-}$ was offered at the time of this early work.[4-7] The dehydrated complex $Fe_2O(ttha)^{2-}$ is more compatible with data from characterization methods that are described in this report. A similar correction in formula from $Fe_2(OH)_2(hedta)_2^{2-}$ to $Fe_2O(hedta)_2^{2-}$ was necessary[8-12] when the oxo-bridged structure for $[enH_2][Fe_2O(hedta)_2]$ was established by Lippard's X-ray evidence.[12]

$Fe^{II}_2(ttha)^{2-}$ undergoes a rapid oxidation with O_2, forming $Fe_2O(ttha)^{2-}$. When first-row transition-metal centers are bridged by a μ-oxo ligand as in **1B**, the metal centers reside about 3.6 Å apart. This distance is comparable to the separation in binuclear metalloproteins such as the non-heme O_2 carrier hemerythrin. EXAFS data of Stern et al. show the Fe(III) centers of oxyhemerythin to be at 3.57-Å separation.[13] The oxo-bridged Fe(III) centers of the oxy or met forms are disrupted in the deoxyhemerythrin Fe(II) form;[13,14] the centers are closer at 3.13 Å in the reduced form, and the oxo bridge is broken. Resonance Raman spectroscopy was used by Klotz et al. to deduce an asymmetric binding of O_2 in one of two possible structures (Figure 1).[15] Single-crystal spectra and EXAFS data support binding of O_2 to only one Fe center.[13,14,16] The Fe(III) centers are ligated by relatively hard donor ligands: five histidine (N) donors, two bridging carboxylate donors (glu, asp), and the oxo group.[14] Two hydroxy groups, one per Fe center, are proposed for the deoxyhemerythrin case in place of the oxo bridge.[13]

Polyamino carboxylate ligands such as $edta^{4-}$, $hedta^{3-}$, and $ttha^{6-}$ provide a set of N and O donors reasonably similar to those of hemerythrin.[17,18] The UV–visible absorption spectrum of $[Fe_2O(hedta)_2^{2-}]$ is very similar to that of methemerythrin.[17-19] Data presented in this paper show that the $Fe_2O(ttha)^{2-}$ complex is quite similar to $[Fe_2O(hedta)_2^{2-}]$, therefore extending its relationship to methemerythrin. The side-by-side location of the

(1) Myser, T. K.; Shepherd, R. E. *Inorg. Chem.* **1987**, *26*, 1544.
(2) Fallon, G. D.; Gatehouse, B. M. *Acta Crystallogr., Sect. B: Struct. Crystallogr. Cryst. Chem.* **1976**, *B32*, 71.
(3) Smith, T. D.; Boas, J. F.; Pillrow, J. R. *Aust. J. Chem.* **1974**, *27*, 2535.
(4) Schroder, K. H. *Acta Chem. Scand.* **1965**, *19*, 1797.
(5) Harju, L. *Anal. Chim. Acta* **1970**, *50*, 475.
(6) Harju, L.; Ringbom, A. *Anal. Chim. Acta* **1970**, *49*, 221.
(7) Bohigan, T. A.; Martell, A. E. *J. Inorg. Nucl. Chem.* **1967**, *29*, 453.
(8) Gustafson, R. L.; Martell, A. E. *J. Phys. Chem.* **1963**, *67*, 576.
(9) Schugar, H.; Walling, C.; Jones, R. B.; Gray, H. B. *J. Am. Chem. Soc.* **1967**, *89*, 3712.
(10) Schugar, H. J.; Rossman, G. R.; Barraclough, C. G.; Gray, H. B. *J. Am. Chem. Soc.* **1972**, *94*, 2683.
(11) Wilkins, R. G.; Yelin, R. E. *Inorg. Chem.* **1969**, *8*, 1470.
(12) Lippard, S. J.; Schugar, H.; Walling, C. *Inorg. Chem.* **1967**, *6*, 1825.
(13) (a) Elam, W. T.; Stern, E. A.; McCallum, J. D.; Saunders-Loehr, J. *J. Am. Chem. Soc.* **1983**, *105*, 1919. (b) Elam, W. T.; Stern, E. A.; McCallum, J. D.; Sanders-Loehr, J. *J. Am. Chem. Soc.* **1982**, *104*, 6369.
(14) (a) Stenkamp, R. E.; Sieker, L. C.; Jensen, L. H. *J. Am. Chem. Soc.* **1984**, *106*, 618. (b) Stenkamp, R. E.; Jensen, L. H. *Adv. Inorg. Biochem.* **1979**, *1*, 219. (c) Hendrickson, W. A. In *Invertebrate Oxygen-Binding Proteins: Structure, Active Site, and Function*; Lamy, J., Lamy, J., Eds.; Dekker: New York, 1981; pp 503-515.
(15) Kurtz, D. M.; Shriver, D. F.; Klotz, I. M. *J. Am. Chem. Soc.* **1976**, *98*, 5033.
(16) Stenkamp, R. E.; Sieker, L. C.; Jensen, L. H.; Sanders-Loehr, J. *Nature (London)* **1981**, *291*, 263.
(17) Okamura, M. Y.; Klotz, I. M. In *Inorganic Biochemistry*; Eichorn, B. G., Ed.; Elsevier: New York, 1973.
(18) Murray, K. S. *Coord. Chem. Rev.* **1974**, *12*, 1.
(19) Gray, H. B. *Adv. Chem. Ser.* **1971**, *No. 100*, 365.

0020-1669/88/1327-0916$01.50/0

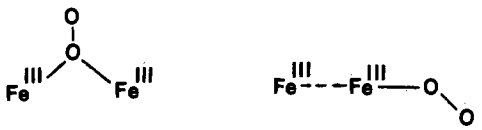

Figure 1. Hemerythrin dioxygen binding compatible with its resonance Raman spectrum.[15]

Fe(III) centers in $Fe_2O(ttha)^{2-}$ provides an interesting comparison for hemerythrin's active site. A simple molecular model shows the Fe–O–Fe angle is less strained for $Fe_2O(ttha)^{2-}$.

Lippard's group has recently prepared a close structural match for the active site of hemerythrin using the self-assembly of a primitive $Fe_2O(O_2CR)_2^{2+}$ core.[20-23] The $[Fe_2O(O_2CR)_2]^{2+}$ core may be ligated at the remaining sites of the Fe(III) centers by N donors (L = hydrotris(1-pyrazolyl)borate anion ($HB(pz)_3^-$) or the cyclic saturated N donor 1,4,7-triazacyclononane (tach or [9]-aneN$_3$)). This coordination yields $[Fe^{III}_2O(L)_2(O_2CR)_2]$ complexes with spectral parameters very similar to those of methemerythrin.

Although the Lippard model is available for structural aspects of the hemerythrin core, few models have been described for the mechanism of oxygenation. Data in this paper show that $Fe^{II}_2(ttha)^{2-}$ reduces O_2 by an inner-sphere pathway. The mechanism of this process may be of interest in regard to the hemerythrin oxygenation.

The species that are produced during O_2 activation by Fe^{II} polyamino carboxylates are also relevant to the action of the Dervan-type DNA nicking complex, MPE–Fe^{II},[24] and to bleomycin drugs used in chemotherapy.[25] MPE–Fe^{II} has an Fe^{II}(edta) unit covalently linked to a methidium bromide moiety. The latter serves as an intercalator between DNA base pairs. The tethered Fe^{II}(edta) unit is then controlled in terms of approach to the DNA chain. Its oxidation by O_2 produces nicking at points along the DNA chain. The mechanism of action has been interpreted as due to a diffusible O_2^- or HO•, formed from the $Fe^{II}(edta)/O_2$ reaction.[24] Similarly, high-spin Fe^{II} complexes in bleomycin and bleomycin analogues activate O_2 in their antitumor action. Ferric superoxo, ferric peroxo, and free HO• species are detectable.[25] In this paper we report kinetic and spin-trapping experiments on the $Fe^{II}_2(ttha)^{2-}/O_2$ reaction, which give interesting contrasts to the O_2 activation schemes proposed for the Dervan-type complexes and the bleomycins.

Experimental Section

Reagents. $H_2{}^{18}O$ water was obtained from Stohler in 99% purity. $Fe(NH_4)_2(SO_4)_2{\cdot}6H_2O$ was obtained from J. T. Baker Chemical Co. Triethylenetetraminehexaacetic acid, H_6ttha, was obtained from Sigma. The DMPO radical trap[26] was obtained from Aldrich. The enzymes, bovine blood superoxide dismutase (SOD) and bovine liver catalyase (CAT), were obtained from Sigma. These enzymes were maintained in the frozen state until immediately prior to use. Solutions were prepared at 0.10 M ionic strength with NaCl and adjusted to near pH 7. O_2, N_2, and Ar gases were supplied by Air Products. N_2 and Ar gases, used to provide inert-atmosphere blanketing gases over the solutions having air sensitivity, were purified by passage through Cr(II) scrubbing towers followed by a H_2O rinse tower. Transfers of air-sensitive solutions were carried out with gastight syringe techniques, using stainless steel needles. O_2 solutions of desired concentrations were obtained by dilution of O_2-saturated H_2O with Ar-purged H_2O.

UV–Visible Spectra. UV–visible spectral data were recorded on a Varian-Cary 118C spectrophotometer. Quartz cells were sealed with rubber septa and flushed with Ar prior to filling with Ar-sensitive solutions.

Infrared Data. Spectra were recorded with an IBM IR/32 FTIR instrument on KBr pellets of the solid complexes prepared as described elsewhere.[39] Raman spectra were recorded by using a SPEX 1403 double monochromator at the 5145-Å emission of an Ar laser. Samples were prepared in H_2O and mounted in a glass capillary tube. The spectra were scanned at 140-mW power at 0.50 s/2 cm^{-1}.

Kinetic Studies. Kinetic data for the reaction between O_2 and $Fe^{II}_2(ttha)^{2-}$ were collected on a Durrum D-110 stopped-flow spectrophotometer interfaced with a DEC-1103 computer for data analysis. Data reduction and analysis were achieved by using appropriate first-order kinetic programs.

Radical-Trapping Experiments. 5,5-Dimethyl-1-pyrroline *N*-oxide (DMPO) was employed. A stock solution of 4.5×10^{-2} M DMPO was made by sampling 0.05 mL of DMPO with a gastight syringe in a glovebag under N_2 and then injecting the DMPO into 10.0 mL of deoxygenated water in a bubbler on the Ar gas line. The DMPO solution was stored under a continuous stream of Ar and transferred to the reaction mixtures by using gastight syringes. A stock solution of 3.0×10^{-3} M $Fe_2(ttha)^{2-}$ at pH 7.2 was also stored under a continuous stream of Ar. For experiments involving H_2O_2 as the oxidizing agent, the reaction mixtures were made by transferring 2.5 mL of the DMPO stock solutions to a deoxygenated solution of 1.0 mL of 3% H_2O_2 (and 0.5 mL of ethanol when appropriate). A 2.5-mL portion of $Fe_2(ttha)^{2-}$ solution was added to the reaction mixture, and the solution immediately became orange. A portion of the reaction mixture was transferred to a deoxygenated flat quartz EPR cell and mounted in the Varian E-4 instrument. The manipulations required about 3 min. When O_2 was used as the oxidizing agent, the reaction mixture was made by combining appropriate amounts of $Fe_2(ttha)^{2-}$, DMPO solution, and deoxygenated ethanol and water under an inert atmosphere. The reaction mixture was oxidized by bubbling a continuous stream of O_2 through the solution for 15 s followed by 2.5–3 min of vigorously bubbling Ar through the solution to purge excess O_2. A portion of the reaction mixture was transferred to the deoxygenated EPR cell and mounted in the instrument within 6 min of when O_2 was first introduced to the system.

$[Me_2Dabco][Fe_2{}^{18}O(ttha)]{\cdot}x\,H_2{}^{18}O$. $[Me_2Dabco][Fe_2{}^{16}O(ttha)]{\cdot}6H_2{}^{16}O$ was prepared by O_2 oxidation of $Fe_2(ttha)^{2-}$ in water of normal isotopic abundance in the presence of $[Me_2Dabco]Cl_2$. Precipitation was induced by reducing the solubility of the desired salt with dimethylformamide. The isolated complex was recrystallized by using the vapor-diffusion method described below. Six waters of hydration were found by using analytical data (Galbraith) and by determining the effective molecular weight and the observed absorbance at 470 nm (ϵ/Fe = 80 M^{-1} cm^{-1}). The resulting solid was examined by infrared spectrophotometry. Samples of ca. 0.013 g of the naturally abundant ^{16}O-labeled $[Me_2Dabco][Fe_2O(ttha)]{\cdot}6H_2O$ were dissolved in 0.50-mL aliquots of $H_2{}^{16}O$, and $H_2{}^{18}O$ was placed in 10.0-mL centrifuge tubes. The oxo-bridged complex (as shown by data herein) was converted to the open-chain form by addition of 0.075 mL of ~1.0 HCl. The solution became yellow upon opening of the bridged complex to the labile open-chain form. Experiments on larger samples show the pH to be about 2 under these conditions. Ten minutes was allowed to ensure complete exchange with the solvent. $Na^{16}OH$ and $Na^{18}OH$ solutions were prepared by the reaction of sodium metal with $H_2{}^{16}O$ and $H_2{}^{18}O$, respectively. The respective $Na^{16}OH$ or $Na^{18}OH$ solution was used to readjust the pH of open-chain-containing solutions. The brown-red color of $Fe_2O(ttha)^{2-}$ reappeared in each case. The desired solids as Me_2Dabco^{2+} salts of $Fe_2O(ttha)^{2-}$ were obtained by addition of 1.50 mL of absolute ethanol to each sample with continuous agitation of the centrifuge tubes.

(20) Armstrong, W. H.; Spool, A.; Papaefthymiou, G. C.; Frankel, R. B.; Lippard, S. J. *J. Am. Chem. Soc.* **1984**, *106*, 3653.
(21) Armstrong, W. H.; Lippard, S. J. *J. Am. Chem. Soc.* **1984**, *106*, 4632.
(22) Spool, A.; Williams, I. D.; Lippard, S. J. *Inorg. Chem.* **1985**, *24*, 2156.
(23) Armstrong, W. H.; Lippard, S. J. *J. Am. Chem. Soc.* **1985**, *107*, 3730.
(24) (a) Hertzberg, R. P.; Dervan, P. B. *J. Am. Chem. Soc.* **1982**, *104*, 313. (b) Schultz, P. G.; Dervan, P. B. *J. Am. Chem. Soc.* **1983**, *105*, 7748.
(25) (a) *Bleomycin: Chemical, Biological and Biological Aspects*; Hecht, S. M., Ed.; Springer: New York, 1979. (b) Sugiura, Y.; Takita, T.; Umezawa, H. In *Metal Ions in Biological Systems*; Dekker: New York, 1985; Vol. 19, p 81.
(26) DMPO = 5.5-dimethyl-1-pyrroline *N*-oxide.
(27) Zhang, S.; Myser, T. K.; Shepherd, R. E., to be submitted for publication in *Inorg. Chem.*
(28) Johnson, C. R.; Shepherd, R. E. *Inorg. Chem.* **1983**, *22*, 3506.
(29) Sievers, R. E.; Bailar, J. C. *Inorg. Chem.* **1962**, *1*, 174.
(30) Nakamoto, K. *Infrared and Raman Spectra of Inorganic and Coordination Compounds*, 3rd ed.; Wiley: New York, 1978.
(31) San Filippo, J.; Grayson, R. L.; Sniadoch, H. J. *Inorg. Chem.* **1976**, *15*, 269.
(32) Wing, R. M.; Callahan, K. P. *Inorg. Chem.* **1969**, *8*, 371.
(33) Hewkin, D. J.; Griffith, W. P. *J. Chem. Soc. A* **1966**, 472.
(34) Cotton, F. A.; Wing, R. M. *Inorg. Chem.* **1965**, *4*, 867.
(35) Wollman, R. G.; Hendrickson, D. N. *Inorg. Chem.* **1977**, *16*, 723.
(36) Ziolo, R. F.; Stanford, R. H.; Rossman, G. R.; Gray, H. B. *J. Am. Chem. Soc.* **1974**, *96*, 7190.
(37) Weaver, T. R.; Meyer, T. J.; Adeyemi, S. A.; Brown, G. M.; Eckberg, R. P.; Hatfield, W. E.; Johnson, E. C.; Murray, R. W.; Untereker, D. *J. Am. Chem. Soc.* **1975**, *97*, 3039.
(38) Fife, D. J.; Moore, W. M. *Photochem. Photobiol.* **1979**, *29*, 43.
(39) Myser, T. K. Ph.D. Thesis, University of Pittsburgh, 1986.

The solid which precipitated in the solution was collected by centrifugation. The water/ethanol solution was decanted, and the solid was resuspended in 1.5 mL of absolute ethanol by stirring with a clean glass rod. The solid products were again isolated by centrifugation. The ethanol phase was removed by pipet, and the moist solids were placed in a desiccator. The remaining ethanol was removed by pumping under vacuum for 30 min. The solids were stored under vacuum overnight. Pellets were prepared in KBr, and infrared spectra were obtained both for the recycled ^{16}O-labeled complex and for the ^{18}O-labeled derivative.

Extended Form: $[Fe_2(H_2O)_2(ttha)]\cdot xH_2O$. The procedure to isolate the extended form of the $Fe^{III}_2(ttha)$ complex was the same as used to form the opening of the bridged complex as described in preparing the ^{18}O-labeled $[Me_2Dabco][Fe_2{}^{18}O(ttha)]\cdot xH_2O$ complex. However, the precipitation step with ethanol was introduced without readjustment of the pH above 4.5. A lemon yellow product was obtained by drying under vacuum as described in the ^{18}O-labeling studies. A slight discoloration toward brownish pink was observed for the dried solution, which had been pumped for 15 h. This suggests some formation of the oxo-bridged form during the drying process of the lemon yellow open-chain derivative. A sample dried by air after using ethanol and diethyl ether washes did not show any surface decolorization.

X-ray Diffraction Studies on $Fe_2O(ttha)^{2-}$. Attempts to grow suitable single crystals containing the $Fe_2O(ttha)^{2-}$ moiety were made by using the following counterions: Me_2Dabco^{2+}, $(CH_3)_4N^+$, $(CH_3CH_2)_4N^+$, $(C_6H_5)_4As^+$, Mg^{2+}, Ca^{2+}, Ba^{2+}, Zn^{2+}, K^+, and Na^+. Only Me_2Dabco^{2+} gave single crystals by the method of vapor diffusion of a 50/50 volume % propylene glycol and 2-propanol mixture into a 2.0-mL solution containing 0.05 M $Fe_2O(ttha)^{2-}$ and 0.05 M Me_2Dabco^{2+}.

X-ray diffraction data were collected with the assistance of J. Abola on a Nicolet P3 four-circle diffractometer using a graphite-monochromated molybdenum X-ray source at room temperature and a θ–2θ scan. Two crystals were employed. The first crystal suffered X-ray damage and/or efflorescence soon after starting to collect data. The second crystal was mounted in a capillary tube with the mother liquid. Although the crystal survived longer, the time was insufficient to collect a complete data set.

It may be inferred that the crystal has large cell dimensions and gives overlapping diffraction points which indicate the data should be collected by using copper radiation. It is still unclear whether the crystal is suffering radiation damage of the Fe(III)–ttha components or just losing solvent molecules during data collection. Since the crystal mounted in the capillary tube lasted much longer than the crystals with solvent protection in a capillary, it appears the crystal is sensitive to solvent loss.

Mössbauer Spectroscopy. The Mössbauer spectrum of $[Me_2Dabco][Fe_2O(ttha)]\cdot 6H_2O$ was obtained with a scanned-velocity spectrometer operating in the time mode. The experimental details and equipment have been described previously by Johnson and Shepherd.[28] A final record of the spectrum was obtained from a printer terminal. Peak positions were also determined directly from the oscilloscope display of the multichannel analyzer. The velocity scale and isomer shift references were obtained by calibration with a sodium nitroprusside (NP) absorber standard. The source was ^{57}Co in a rhodium matrix.

Results and Discussion

Nature of Fe(II) and Fe(III) Binuclear Complexes in Solution. Fe(II) and Fe(III) binuclear $ttha^{6-}$ complexes are fully formed in solution.[4-7] The log β_2 constants for formation of the binuclear complexes are 27.3 for Fe(II)[4] and 40.5 for Fe(III).[5] The conditional stability constants are such that less than 10^{-3}% of $Fe^{II}_2(ttha)^{2-}$ or 10^{-5}% of the Fe(III) binuclear complex is dissociated at pH >4.0.[4-7] The similarity in spectra and properties described in subsequent sections for the Fe(III)–ttha binuclear complex compared to those of $Fe_2O(hedta)_2^{2-}$ support the formula $Fe_2O(ttha)^{2-}$ for the Fe(III) derivative. No significant hydrolysis with increasing pH is observed for the $Fe^{II}_2(ttha)$ complex. This requires at least one labile H_2O molecule per Fe(II) coordination site up to pH 10 in order to conserve six donors per Fe(II) center. One replaceable H_2O per Ru(II) has been established in our laboratories for the related $Ru_2(H_2O)_2(ttha)^{2-}$ complex.[27]

UV–Visible Spectra of Fe(II) and Fe(III) $ttha^{6-}$ Complexes. A colorless solution resulted when equimolar amounts of $Fe(NH_4)_2(SO_4)_2\cdot 6H_2O$ and H_3hedta were mixed under N_2 and the pH was adjusted to 6.86. Upon exposure to oxygen the solution turned orange and had an absorption peak at 475 nm identical with that of $[Fe(hedta)]_2O^{2-}$.[9,10] This visible band at 475 nm (ϵ = 180 M^{-1} cm^{-1})[1] has been assigned as a ligand-field band $\{^6A_1 \rightarrow [^4A_1, {}^4E]({}^4G)\}$.[9]

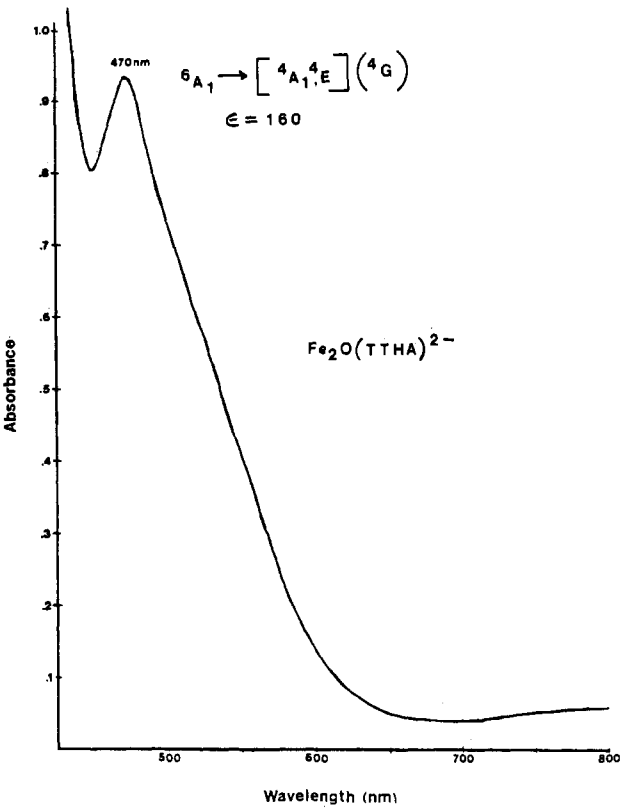

Figure 2. Visible spectrum of $Fe_2O(ttha)^{2-}$: $[Fe_2O(ttha)^{2-}] = 5.84 \times 10^{-3}$ M; pH 7.2; μ = 0.05; T = 25.0 °C.

A colorless solution also results when Fe(II) is mixed 2:1 with $ttha^{6-}$. Upon exposure to oxygen the solution becomes dark orange and has an absorption band with a peak at 470 nm; ϵ/Fe = 80 M^{-1} cm^{-1} (Figure 2). The features are the same as for $[Fe_2O(hedta)_2^{2-}]$. The complex may be adsorbed onto an anion-exchange resin and eluted with 2M NaCl. This is consistent with the 2– charge of $Fe_2O(ttha)^{2-}$. This formula is also consistent with the 8 mol of OH^- consumed in the titration forming the binuclear Fe(III)[4-7] species and with the spectral similarity to the oxo-bridged complexes $[Fe(hedta)]_2O^{2-}$ and $V_2O(ttha)^{2-}$.[1]

Infrared Studies of Metal $ttha^{6-}$ and $hedta^{3-}$ Complexes. Infrared spectra of metal complexes with edta-type ligands exhibit stretching frequencies of the carbonyl group of the carboxylates as follows: coordinated carboxylate, –COOM (1650–1590 cm^{-1}); pendant ionized carboxylates, $-COO^-$ (1610–1575 cm^{-1}); pendant protonated carboxylates, –COOH (1750–1700 cm^{-1}).[29,30] $Me_2Dabco[Fe_2{}^{16}O(ttha)]\cdot 6H_2O$ exhibits a single sharp peak at 1630 cm^{-1} (Figure 3-2). The open-chain form (Figure 3-1) has only one such stretch at 1647 cm^{-1}. This indicates that all the carboxylate moieties are coordinated to the ferric ions of $Fe_2O(ttha)^{2-}$ or $Fe_2(ttha)(H_2O)_2$. Schugar et al.[9] observed a single sharp peak around 1630 cm^{-1} in $(enH_2)[Fe_2O(hedta)_2]$, which is also observed by X-ray methods to have no uncoordinated carboxylate groups.[12] A Raman spectrum of $Fe_2O(ttha)^{2-}$ in H_2O exhibits only a single band centered at 1628 cm^{-1} (Figure 1SM in supplementary material).

The use of infrared data to determine the presence or absence of an oxo bridge between two transition-metal atoms is a more complicated matter. Complexes possessing a single oxo bridge are expected to have two observable IR bands, a symmetric stretch (ν_{sym}) and an asymmetric stretch (ν_{asym}). The asymmetric stretch should be at substantially higher frequency than the symmetric stretch, but the frequencies are very sensitive to the M–O–M bond angle.[31,32] For bent M–O–M systems, the symmetric stretch occurs at higher frequencies and the asymmetric stretch occurs at lower frequencies than for linear M–O–M systems.[31,34] The position of the symmetric stretch is potentially more informative since it is believed to reflect more directly the M–O–M angle; however, this band remains ill characterized. Although a number of IR

Table I. Selected Infrared Peaks[a]

complex	C=O str, cm^{-1}	peaks between 900 and 700 cm^{-1}					
$[Me_2Dabco][Fe_2O(ttha)]\cdot 6H_2O$	1630	868	833	816		733	
$[Fe_2(ttha)(H_2O)_2]$	1647	866		817		734	
$Mg[Fe_2O(ttha)]$	1622	868	839	818		735	
$Na_2[V_2O(ttha)]$	1636	868		818		740	
$Na_2[(VO)_2(ttha)]$	1640	874		820	783	747	725
$Mn_2(ttha)$	1588	853		815		722	
$Mg[Ni_2(ttha)]$ "oil"	1597	870		814		733	
$Mg[Ni_2(ttha)]$ "crystal"	1601	870		821	781	735	725
$[Cr(hedta)(H_2O)]$	1640	874		816		750	733
$[Ti(edta)(H_2O)]$	1701	874		835		743	719
$K[Co(edta)]\cdot 2H_2O$	1651	887		850	774	736	

[a] Solids isolated as described in ref 39 or in the Experimental Section.

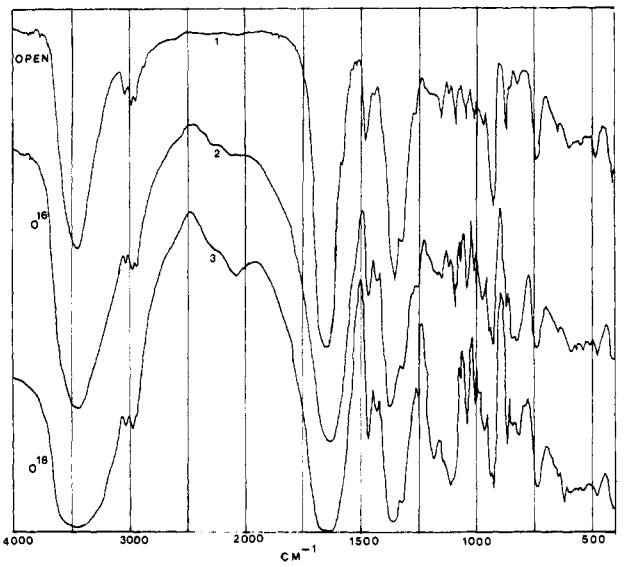

Figure 3. Infrared spectra of $[Me_2Dabco][Fe_2O(ttha)]$: (1) $Fe_2(ttha)(H_2O)_2$; (2) $[Me_2Dabco][Fe_2O(ttha)]\cdot 6H_2O$; (3) ^{18}O-labeled $[Me_2Dabco][Fe_2O(ttha)]\cdot 6H_2{}^{18}O$. Solids are isolated as described in the Experimental Section.

studies on oxo-bridged metal complexes have been done,[31-34] there is still little correlation between the appearance of the bands and the M–O–M angle. It is generally agreed that the asymmetric stretch for linear M–O–M systems is found between 800 and 900 cm^{-1} and that bending of the M–O–M linkage lowers the asymmetric stretching frequency to the 700–800-cm^{-1} range. However, the absence of a band in the 700–900-cm^{-1} region does not necessarily rule out the presence of an oxo bridge. Several systems with oxo bridges, such as Hendrickson's Fe(III)–Fe(IV) oxo-bridged porphyrin,[35] Gray's Mn(III)–O–Mn(III) porphyrin,[36] and Meyer's $Cl(bpy)_2Ru–O–Ru(bpy)_2Cl^{n+}$ complexes[37] exhibit no strong absorptions in the 700–900-cm^{-1} region that they could assign to the asymmetric stretch.

Table I lists infrared bands in the 700–900-cm^{-1} region for $ttha^{6-}$, $hedta^{3-}$, and $edta^{4-}$ complexes. On the basis of the IR spectra, only one of these compounds may be unequivocally assigned as having an asymmetric stretch of the M–O–M linkage. All the $ttha^{6-}$ complexes have at least two infrared bands between 800 and 900 cm^{-1}. They all have a strong sharp band around 870–880 cm^{-1} and a weaker band around 818 cm^{-1}. Similar bands are also observed in the $hedta^{3-}$ and $edta^{4-}$ complexes studied. In the IR spectrum of $[Fe_2O(ttha)]^{2-}$, a third band appears in the 800–900-cm^{-1} region (Figure 3-2). This band was observed at 833 cm^{-1} in a sample from crystals with Me_2Dabco^{2+} as the counterion and 839 cm^{-1} in a sample from crystals with Mg^{2+} as the counterion. The oxo-bridged dimers of Fe(III)–edta and Fe(III)–hedta both have an infrared band at 830 cm^{-1}, which has been assigned as the Fe–O–Fe asymmetric stretch.[12] It is surprising that ν_{asym} for $Fe_2O(ttha)^{2-}$ appears at nearly the same frequency as the linear oxo-bridged dimers since $Fe_2O(ttha)^{2-}$ is expected to be bent and observed at lower frequency. The additional rigidity imposed by the ethylene bridge may, however, cause the frequency of this vibration to be higher than expected.

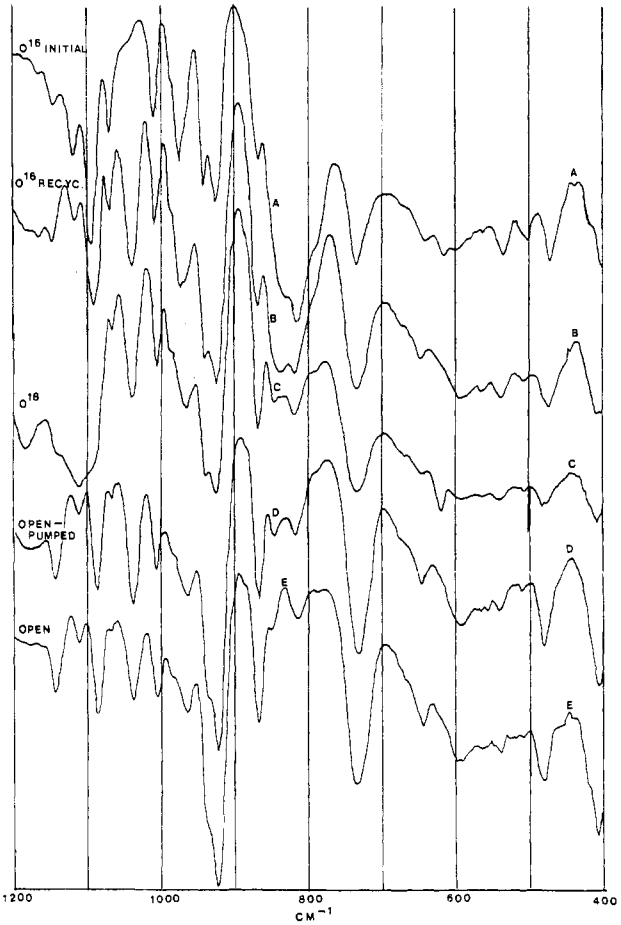

Figure 4. Infrared region from 1200 to 400 cm^{-1}: (A) original $[Me_2Dabco][Fe_2O(ttha)]\cdot 6H_2O$ complex; (B) original sample carried through oxo-bridge opening and closing procedure in $H_2{}^{16}O$; (C) original sample treated as in (B) in $H_2{}^{18}O$; (D) original sample opened at pH ~2 and dried 15 h under vacuum; (E) original sample opened at pH ~2 and dried by ethyl ether at atmospheric pressure. All isolation procedures are as described in the Experimental Section.

The assignment of the 833-cm^{-1} band to the Fe–O–Fe asymmetric stretch is confirmed by the ^{18}O-labeled $[Me_2Dabco][Fe_2{}^{18}O(ttha)]\cdot H_2{}^{18}O$ solid (Figure 3-3). The isolation procedure is described in the Experimental Section. The ^{18}O-labeled compound exhibits a reduction in intensity of both the 816-cm^{-1} stretch and its higher energy shoulder (833 cm^{-1} for the ^{16}O natural isotope). The ^{18}O-labeled compound exhibits bands at 846 and 817 cm^{-1} at much reduced intensity. All other bands in the 1100–400-cm^{-1} region remained unchanged. These results are shown in Figure 4A for the originally isolated $[Me_2Dabco][Fe_2{}^{16}O(ttha)]\cdot 6H_2O$ solid, Figure 4B for the ^{16}O complex, which is taken through the ring-opening/ring-closure procedure without

Table II. Rate Data from the $Fe^{II}_2(ttha)^{2-}/O_2$ Reaction[a]

[H+], M	rate, M^{-1} s^{-1}	rate − 63, M^{-1} s^{-1}	1/[H+], M^{-1}	1/rate, M s
1.95×10^{-6}	274.0	211	5.13×10^{5}	4.74×10^{-3}
1.76×10^{-6}	255.0	192	5.75×10^{5}	5.21×10^{-3}
9.30×10^{-7}	242.0	179	1.07×10^{6}	5.59×10^{-3}
8.90×10^{-7}	233.0	170	1.12×10^{6}	5.88×10^{-3}
5.2×10^{-7}	232.0	169	1.91×10^{6}	5.92×10^{-3}
5.1×10^{-7}	228.0	165	1.95×10^{6}	6.06×10^{-3}
3.2×10^{-7}	207.0	144	3.09×10^{6}	6.94×10^{-3}
2.0×10^{-7}	196.0	133	5.0×10^{6}	7.52×10^{-3}
1.9×10^{-7}	161.0	98	5.37×10^{6}	1.02×10^{-2}
1.20×10^{-7}	153.6	90.6	8.13×10^{6}	1.10×10^{-2}
9.33×10^{-8}	135.0	72.0	1.07×10^{7}	1.39×10^{-2}
5.89×10^{-8}	126.0	63.0	1.70×10^{7}	1.59×10^{-2}
4.79×10^{-8}	129.0	66.0	2.09×10^{7}	1.52×10^{-2}
1.91×10^{-8}	83.5	20.5	5.25×10^{7}	5.0×10^{-2}
1.51×10^{-8}	76.0	13.0	6.61×10^{7}	7.69×10^{-2}
7.94×10^{-9}	63.0	0	1.26×10^{8}	

[a] T = 25.0 °C; μ = 0.01.

change, Figure 4C for the ^{18}O-labeled product (≥80% ^{18}O), Figure 4D for the solid isolated at pH ~2 as the open-chain $[Fe_2(ttha)(H_2O)_2]$ complex and dried for 15 h under vacuum, and Figure 4E for the open-chain complex isolated and dried by an ethyl ether rinse followed by rapid air-drying. The 833-cm^{-1} band is lost, caused by either the ^{18}O-labeling or formation of open-chain complex. Residual bands at 868, 846, and 817 cm^{-1} for the open-chain complex (Figure 4D,E) are comparable to bands at slightly lower frequency for the H_6ttha ligand itself or to those of the open-chain $Na_2[Ru^{II}_2(ttha)(H_2O)_2]$ solid.[27] The ^{18}O-labeled complex showed no bands at lower frequency than could be reassigned as the Fe–^{18}O–Fe asymmetric stretch; the visible spectrum for the ^{18}O-labeled complex was equivalent to the initial ^{16}O natural complex in the oxo-bridged form. All of the complexes that were isolated by precipitation with absolute ethanol exhibited a band at 1040 cm^{-1} that was absent in the starting material (cf. Figure 4A vs Figure 4B–E); this is assigned to the ν_{C-O} of ethanol.

None of the other complexes in Table I had any bands in the infrared region that we could assign as the M–O–M asymmetric stretch. Even $V_2O(ttha)^{2-}$, which is oxo bridged in solution, had only two bands between 800 and 900 cm^{-1}. $V_2O(ttha)^{2-}$ is strained and probably has a bent V–O–V linkage, which would give an asymmetric stretch between 700 and 800 cm^{-1}.[1] The complex does have a broad IR band centered at 740 cm^{-1}; it is not yet possible to determine if this band can be attributed to the V–O–V linkage because the ^{18}O-labeling study has not been done. The V(IV) dimer and Cu(II) dimer are known to be in an extended-chain arrangement (unbridged) in the solid state.[2,40] The V(IV) dimer has three bands between 700 and 800 cm^{-1}, so there is no clear correlation between structure and the number of bands in this region. It is also possible that, like $(VO)_2(ttha)^{2-}$ and $Cu^{II}_2(ttha)^{2-}$, $V_2O(ttha)^{2-}$ may be oxo bridged in solution and unbridged in the solid state, but the color of the solid argues against this possibility. The inability to assign an asymmetric M–O–M stretch to other $ttha^{6-}$ complexes should not be taken as proof of the absence of an oxo bridge in these complexes. The band may appear in a different region of the spectrum and simply not be identified, or it may be obscured by other bands in the spectrum.

Autoxidation of $Fe_2(ttha)^{2-}$. The rate of the formation of $Fe_2O(ttha)^{2-}$ from the reaction of $Fe^{II}_2(ttha)^{2-}$ and O_2 was studied on the stopped-flow spectrophotometer. The experiments were conducted by using an excess of $Fe_2(ttha)^{2-}$ and monitoring the appearance of the product at 470 nm. Plots of the ln $(A_\infty - A)$ vs time gave straight lines, indicating the reaction is first order in the $Fe^{II}_2(ttha)^{2-}$ complex and O_2.

Table II presents data from a study of the effect of pH on the rate. A plot of the observed second-order rate constant vs $[H_3O^+]$ exhibits rate saturation in hydrogen ion. The rate for the lowest

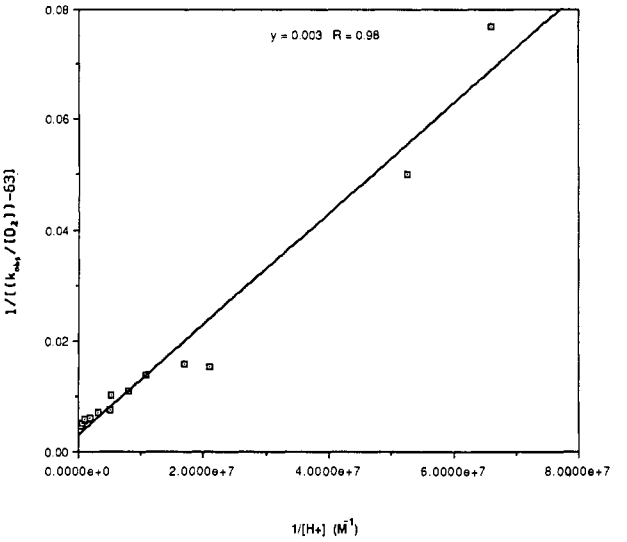

Figure 5. Variations of $Fe_2(ttha)^{2-}/O_2$ reaction with pH.

concentration of hydrogen ion studied was 63 M^{-1} s^{-1}. Data reduction is feasible if one assumes this residual rate is due to a parallel acid-independent pathway. A plot of $1/[(k_{obsd})/[O_2]) - 63]$ vs $1/[H_3O^+]$ gave a straight line, as shown in Figure 5. The data conform to the following rate law where k_0 = 63 M^{-1} s^{-1}:

$$\text{rate} = \frac{d[Fe_2O(ttha)^{2-}]}{dt} = \left(\frac{K_{O_2}k_1k_2[H^+]}{k_{-1} + k_2[H^+]} + k_0\right)[Fe_2(ttha)^{2-}][O_2] \quad (1)$$

The linear fit yields the parameters $K_{O_2}k_1 = 3.32 \times 10^2$ M^{-1} s^{-1} and $k_2/k_{-1} = 3.01 \times 10^6$ M^{-1}.

Enzyme studies were conducted by using superoxide dismutase and catalase as traps for O_2^- and O_2^{2-} in the same manner as was used for the vanadium–ttha system described in a previous paper.[1] Assuming the enzyme-catalyzed dismutation of these anions is faster than the $Fe_2(ttha)^{2-}/O_2^-$ or $Fe_2(ttha)^{2-}/O_2^{2-}$ reactions, the introduction of SOD or catalase would reduce the rate of the $Fe_2(ttha)^{2-}/O_2$ reaction by a factor of 2 if O_2^- or O_2^{2-} were produced outer sphere. This rate assumption has been justified elsewhere for the $V_2O(ttha)^{2-}$ case,[1] and the net rates with $Fe_2(ttha)^{2-}$ are within a factor of 2 of those for $V_2O(ttha)^{2-}$. The validity of the assumption is supported by the additional fact that the rate constants for trapping of O_2^- by SOD and O_2^{2-} by catalase are many orders of magnitude higher than the constants extracted from the tabular rate data. When superoxide dismutase was added to the $Fe_2(ttha)^{2-}/O_2$ system at [SOD] = 1.11×10^{-5} M, no appreciable change in the rate was observed. The rate observed was 0.87 ± 0.04 s^{-1} without the enzyme and 0.77 ± 0.04 s^{-1} with the enzyme. The numbers are within the range of normal experimental variance for the reaction conditions. The reaction rate was also not significantly affected by the addition of catalase at 7.08×10^{-6} M. On the same solution of $Fe_2(ttha)^{2-}$, a rate of 0.33 ± 0.02 s^{-1} was seen without the enzyme, and a rate of 0.44 ± 0.02 s^{-1} was seen when the enzyme was present. These enzyme experiments imply no free superoxide or peroxide is produced during the oxidation of $Fe_2(ttha)^{2-}$ by O_2. The same conclusion may be drawn from spin-trapping studies described in a subsequent section.

The mechanism of the $Fe^{II}_2(ttha)^{2-}/O_2$ reaction must account for several observed features: (1) the rate expression exhibits a proton dependence, which infers a proton-dependent step followed by a previous, reversible step involving O_2; (2) the reaction is inner sphere; no free O_2^-, O_2^{2-}, or $HO^\bullet$ is produced (see spin-trapping section concerning this feature); (3) the reaction is first order in $[Fe_2(ttha)^{2-}]$; (4) the observed rate is significantly slower than a substitution-limited reaction for a labile high-spin Fe(II) complex (ca. 10^5 M^{-1} s^{-1}).[41]

(40) (a) Leverett, P. J. *J. Chem. Soc., Chem. Commun.* **1974**, 161. (b) Smith, T. D.; Martell, A. E. *J. Am. Chem. Soc.* **1972**, *94*, 4123.

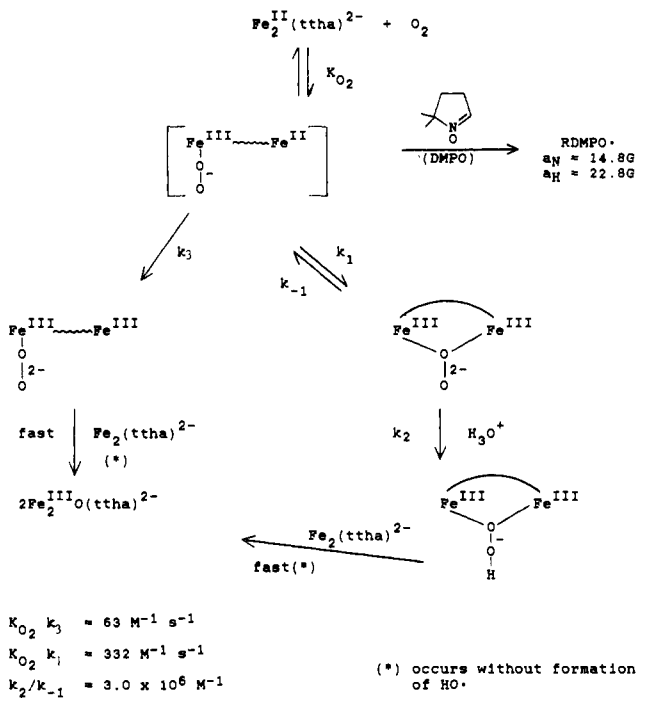

Figure 6. Proposed mechanistic scheme for the autoxidation of $Fe_2(ttha)^{2-}$.

The mechanism shown in Figure 6 is compatible with all of the data. Radical-trapping experiments show the existence of a species with O_2^- activity. This species forms a carbon-centered radical in low yield in competition with the major pathway forming $Fe_2O(ttha)^{2-}$. The radical is similar to one generated by the photooxidation of $dtpa^{5-}$ by O_2 in the presence of riboflavin as a sensitizer, via O_2^- attack of a polyamino carboxylate unit.[38] Two pathways ultimately yield the same $Fe_2O(ttha)^{2-}$ product. One pathway is independent of $[H_3O^+]$ and has a net second-order rate constant of 63 M^{-1} s^{-1}. The other path requires the reversible addition of dioxygen on $Fe^{II}_2(ttha)^{2-}$ followed by a reversible change in this intermediate. Both pathways can be conceived as involving the common initial superoxo intermediate, which is formed by the rapid, reversible addition of O_2 at one of the two open-chain sites of $Fe^{II}_2(ttha)^{2-}$. Two possible events then follow. Either the superoxo intermediate carries out closure to form a bridged peroxo intermediate or the terminal Fe^{II} center of the superoxo intermediate transfers an electron to form a terminal peroxo complex. (Note: A reviewer has expressed preference for either an $Fe^{II}O_2$ or $Fe^{IV}O_2^{2-}$ oxidation-state assignment instead of $Fe^{III}O_2^-$ as we have assigned it here. A resonance of all three forms can explain the overall redox behavior of the two competitive paths.) Outer-sphere reduction of the superoxo intermediate by another $Fe_2(ttha)^{2-}$ molecule is ruled out by the first-order dependence in $Fe_2(ttha)^{2-}$ for both pathways. The structure that is suggested for the peroxo-bridged intermediate in Figure 6 has been made on the basis of the stabilization provided by its reaction with a proton. It could be argued that the peroxo group remains terminally bound to one Fe^{III} center and that the ring closure step involves formation of an oxo-bridged species involving the solvent molecule from the second iron site, e.g.

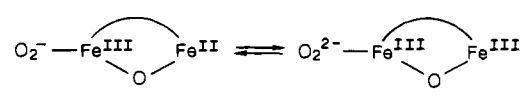

This would be a structure similar to that of hemerythrin in the oxygenated form. However, several things argue against this possibility. There is no separate evidence for a stable (Fe^{III}–O–Fe^{II})(ttha) complex. (See electrochemistry section.) $Fe_2O(ttha)^{2-}$ does not add H_2O_2 at a pH where $Fe_2O(ttha)^{2-}$ is stable (pH >4.5).[42] Therefore, no second labile site is readily available that would be a requirement for a terminal-peroxo intermediate in the proton-dependent pathway. Furthermore, species in which the peroxo anion (HO_2^-) bridges metal centers in the single oxo-like bridging assembly are known in $Co^{III}(O_2H)Cr^{III}$ chemistry.[43] Therefore, the most likely intermediate in the proton-dependent path is as shown in Figure 6. Finally, the fate of the peroxo intermediate by either pathway does not involve a one-electron transfer from Fe^{II}. Such a step would generate HO·, and this species is not trapped by the presence of DMPO. HO· is trapped by DMPO even in the presence of 0.10 M H_2edta^{2-}; therefore, polyamino carboxylates are not good scavengers for HO·[52] in competition with DMPO. The peroxo complexes are rapidly consumed by another mole of $Fe^{II}_2(ttha)^{2-}$ without liberation of HO·. It would seem most facile for an atom-transfer process in the scavenging step if the peroxo species would possess an asymmetric coordination such that the terminal oxygen would be more readily available for the rapid two-electron atom-transfer reaction that consumes the second mole of $Fe_2(ttha)^{2-}$, as required by the overall stoichiometry. If the reviewer's opinion that the open form of the $Fe^{II}_2(ttha)^{2-}/O_2$ intermediate is to be assigned as $Fe^{IV}O_2^{2-}$ at the oxygenated iron site is correct, the atom-transfer path via the k_3 step is facilitated by a relatively easier 2e reduction with atom transfer to a second mole of $Fe^{II}_2(ttha)$. The resulting extended ferryl/ferrous entity would form the $Fe_2O(ttha)^{2-}$ product with ring closure. However ferric peroxo species ($Fe^{III}O_2^{2-}$) are well-known to epoxidize olefins by atom transfer.[61,62] The intermediates shown in Figure 6 are therefore in keeping with prior observations with Udenfriend's reagent.[62]

The ratio of the rate constrant for proton scavenging of the peroxo-bridged complex to that for reopening of the peroxo–Fe^{III} bond (k_2/k_{-1}) is 3.0 × 10^6 M^{-1}. $K_{O_2}k_1$ (332 M^{-1} s^{-1}) is much greater than $k_0 = K_{O_2}k_3$ (63 M^{-1} s^{-1}). At 1 M H_3O^+ there would be a large advantage for the pathway utilizing ring closure to the peroxo-bridged species. However, in the pH domain of 6–7, where the oxo-bridged product is stable, there is a significant competition between the ring-closure proton-dependent path and the pseudo-outer-sphere reduction path. At pH 7, 55% of the reaction occurs via ring closure and 45% by the pseudo-outer-sphere

(41) Calculated by assuming K_{OS} for a neutral water molecule of 0.10 M^{-1} and the water-exchange rate constant of 3 × 10^6 s^{-1}: Swift, T. J.; Connick, R. E. *J. Chem. Phys.* **1962**, *37*, 307.

(42) Shepherd, R. E., unpublished results.
(43) Hyde, M. R.; Sykes, A. G. *J. Chem. Soc., Dalton Trans.* **1974**, 1550.
(44) Janzen, E. G. *Acc. Chem. Res.* **1971**, *4*, 31.
(45) Evans, C. A. *Aldrichimica Acta* **1979**, *12*, 23.
(46) Johnson, C. R.; Shepherd, R. E. In *Mechanistic Aspects of Inorganic Chemistry*; Rorabacher, D. B., Endicott, J. F., Eds.; ACS Symposium Series 198; American Chemical Society: Washington, DC, 1982.
(47) Gilbert, B. C.; Norman, R. O. C.; Sealy, R. C. *J. Chem. Soc., Perkin Trans. 2* **1973**, 2174.
(48) Harbour, J. R.; Chow, V.; Bolton, J. R. *Can. J. Chem.* **1974**, *52*, 3549.
(49) Kremer, M. L. *Isr. J. Chem.* **1971**, *9*, 321.
(50) Harbour, J. R.; Bolton, J. R. *Biochem. Biophys. Res. Commun.* **1975**, *64*, 803.
(51) Suguria, Y.; Takita, T.; Umezawa, H. In *Metal Ions in Biological Systems*; Sigel, H., Ed.; Dekker: New York, 1985; Vol. 19, p 81.
(52) Myser, T. K.; Johnson, C. R.; Shepherd, R. E. *Inorg. Chem.*, in press.
(53) Bancroft, G. M. *Mössbauer Spectroscopy*; McGraw-Hill: New York, 1973; Chapters 5 and 6.
(54) Drago, R. S. *Physical Methods in Chemistry*; Saunders: Philadelphia, PA, 1977; Chapter 15.
(55) McLendon, G.; Motekaitis, R. J.; Martell, A. E. *Inorg. Chem.* **1976**, *15*, 2306.
(56) (a) Stenkamp, R. E.; Jensen, L. H. *Adv. Inorg. Biochemistry* **1979**, *1*, 219–233. (b) Loehr, J. S.; Loehr, T. M. *Ibid.* **1979**, *1*, 235–252.
(57) (a) Okamura, M. Y.; Klotz, I. M. In *Inorganic Biochemistry*; Eichorn, G. L., Ed.; Elsevier: New York, 1973; Chapter 11. (b) Okumura, M. Y.; Klotz, I. M., unpublished resulted quoted in ref 57, p 339.
(58) Wherland, S.; Gray, H. B. In *Biological Aspects of Inorganic Chemistry*; Addison, A. W.; Cullen, W. R., Dolphin, D., James, B. R., Eds.; Wiley: New York, 1977; Chapter 10, p 323.
(59) Zhang, S. S.; Shepherd, R. E., unpublished results.
(60) Zhang, S. S.; Myser, T. K.; Shepherd, R. E. Presented at the 19th Central Regional Meeting of the American Chemical Society, Columbus, OH, June 25, 1987.
(61) Ochiai, E.-I. *Bioinorganic Chemistry, An Introduction*; Allyn and Bacon: Boston, 1977; Chapters 7 and 10.
(62) Udenfriend, S.; Clark, C. T.; Axelrod, J.; Brodie, B. B. *J. Biol. Chem.* **1954**, *208*, 731.

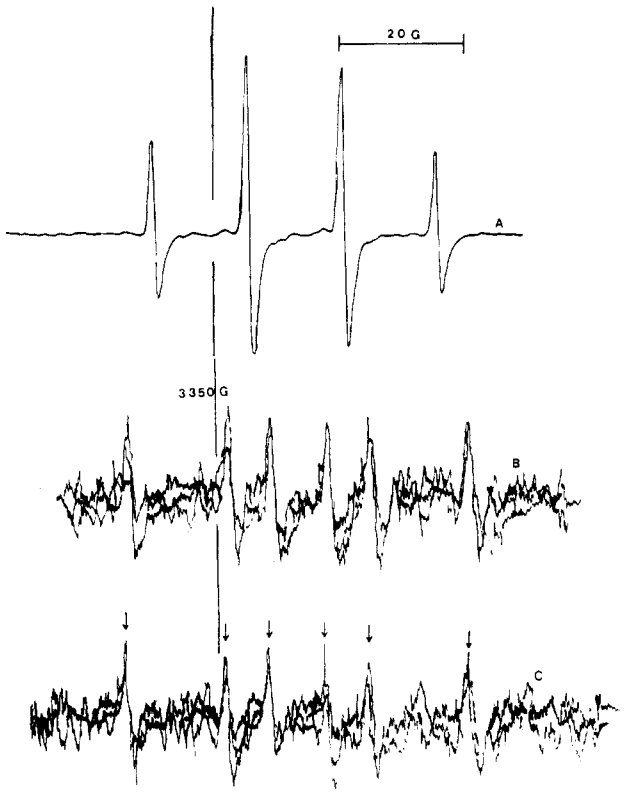

Figure 7. DMPO radical trapping experiments with $Fe_2(ttha)^{2-}$: (A) [DMPO] = 2.25×10^{-2} M, [H_2O_2] = 3.0×10^{-3} M, [$Fe_2(ttha)^{2-}$] = 8.85×10^{-4} M; (B) [DMPO] = 2.25×10^{-2} M, [$Fe_2(ttha)^{2-}$] = 1.48×10^{-3} M, O_2-saturated solution; (C) [DMPO] = 2.05×10^{-2} M, [$Fe_2(ttha)^{2-}$] = 1.34×10^{-3} M, [C_2H_5OH] = 1.56 M, O_2-saturated solution. Conditions: 9.405-GHz frequency, 10.0-mW power, 0.80-G modulation amplitude. Receiver gains: (A) 2.5×10^3; (B, C) 4.0×10^4.

electron-transfer route.

Spin-Trapping Studies of Species in the Reduction of O_2 and H_2O_2 by $Fe_2(ttha)^{2-}$. Spin-trapping studies using DMPO or PBN have proven useful as a diagnostic tool in the detection of intermediates that are produced in O_2 and H_2O_2 reductions. The technique has been reviewed by Janzen[44] and by Evans.[45] DMPO is useful in differentiating between O_2^- and HO•, which are formed in the one-electron reduction sequence of O_2 and H_2O_2, respectively. The spin-trapping method has been applied to metal ion/peroxide reactions,[46-49] to the electron-transport reactions of spinach chloroplasts,[50] and for studies of O_2 activation by bleomycin drugs.[51] The application of the spin-trapping technique as applied to O_2 reduction by $V_2O(ttha)^{2-}$ has been described in detail previously.[1] This reference should be consulted as background information concerning the use of alcohols as mediators in trapping experiments.

Results of prior studies with DMPO and PBN[1,46,52] show that HO• is readily trapped, either in a direct way or with alcohol mediators, when H_2O_2 is reduced by one-electron steps. When O_2^- is generated in an outer-sphere process, either HO_2•, when O_2^- is formed at sufficiently low concentrations, or its HO• decay product, when O_2^- production is high, may be detected by using DMPO. When O_2^- is produced by inner-sphere oxidation of metal centers, no radicals with ESR parameters the same as those of free O_2^- or HO• are detectable.[1,46,52]

DMPO radical trapping experiments were performed as described in the Experimental Section for the $Fe_2(ttha)^{2-}/O_2$ and $Fe_2(ttha)^{2-}/H_2O_2$ reactions at [$Fe_2(ttha)^{2-}$] = (1.5–0.89) $\times 10^{-3}$ M. The results of the DMPO experiments are shown in Figure 7A–C. The $Fe_2(ttha)^{2-}/H_2O_2$ reaction clearly shows the HO• radical adduct of DMPO is detected at high intensity (Figure 7A). The coupling constants $a_N = a_H = 15.0$G, and the 1:2:2:1 pattern is diagnostic of the HO• adduct. When O_2 is used to oxidize $Fe_2(ttha)^{2-}$, a weak, six-line equal-intensity signal is detectable at high receiver gain (Figure 7B). The trapped radical is obviously not •OH. The observed coupling constants $a_N = 14.8$ G and $a_H = 22.8$ G rule out HO_2•. The coupling constants imply that the trapped radical is carbon centered. Experiments with excess ligand present do not show an increase in radical yield; therefore, the C-centered radical results from attack of the coordinated $ttha^{6-}$ ligand. An effort was made to amplify the trapping step by use of ethanol at 1.56 M as an intermediate scavenger (Figure 7C). The observed ESR spectrum ($a_N = 16.0$ G, $a_H = 22.8$ G) was that of the authentic CH_3CHOH adduct of DMPO with coupling constants very close to the literature values ($a_N = 16.2$ G, $a_H = 23.2$ G).[46,52] The intensity of the signal is almost identical with the one observed without the ethanol scavenger. On the basis of the relative intensity of the signals in Figure 7A,B, it is calculated that about 6% of the $Fe_2(ttha)^{2-}/O_2$ reaction results in the carbon-centered radical. Since an outer-sphere reaction with O_2 forming either O_2^- or O_2^{2-} would result in the eventual trapping of the same radical shown in Figure 7A, then the dominant reaction pathway (Figure 6) must proceed by a simple net reduction of dioxygen to water without attack of the parent ligand structure. The main Fe(III) product will be the metal-center-oxidized $Fe_2O(ttha)^{2-}$ product. Confirmatory evidence for the absence of outer-sphere formation of O_2^- and O_2^{2-} was obtained by the absence of any rate suppression in forming $Fe_2O(ttha)^{2-}$ in the presence of either SOD or catalase enzymes (see the kinetic section for the $O_2/Fe_2(ttha)^{2-}$ reaction). The results reported here show that Fe(II) in a polyamino carboxylate environment will attack preferentially oxidizable C_2H_5OH substrate in its primary solvation cage rather than following the "self-attack pathway" shown by the trapped radical species of Figure 7C.

Differential-Pulse Study of $Fe_2(ttha)^{2-}$. Differential-pulse voltammetry was carried out by using the standard three-electrode assembly with a glassy-carbon working electrode and an SCE reference. A 3.00×10^{-3} M solution of $Fe^{II}_2(ttha)(H_2O)_2^{2-}$ was prepared from $Fe(NH_4)_2(SO_4)_2 \cdot 6H_2O$. This was diluted to 1.50×10^{-3} M with 6.86 M phosphate buffer. Only a single differential-pulse wave was detected at +0.022 V vs NHE. The operational pH was 6.41. $E_{1/2}$ for $Fe^{III/II}(edta)^{-/2-}$ is reported to be 0.120 V vs NHE.[58] Therefore the electrochemical behavior for $Fe^{II}_2(ttha)^{2-}$ and $Fe^{II}(edta)^{2-}$ is very similar. No stable II,III species that undergoes a second 1e oxidation is observed. This suggests both iron centers are oxidized at nearly the same potential, independently. No wave from −0.26 to −0.74 V (vs NHE) was observed for the $Fe^{III}_2O(ttha)^{2-}$ oxidation product after passage of O_2 through the original solution for 30 min. Absence of a reduction wave suggests (Fe^{III}–O–Fe^{II})(ttha) is not a stable complex. Furthermore, attempts to prepare the mixed-oxidation-state III,II complex by sequential addition of 1 equiv/$ttha^{6-}$ of Fe(II) and Fe(III) have always resulted in rapid rearrangement to form 0.5 equiv of $Fe_2O(ttha)^{2-}$.[59] A similar metal-exchange reaction occurs when [Cu^{II},Fe^{II}(ttha)] is oxidized by O_2; Cu_2(ttha)$^{2-}$ and $Fe_2(ttha)^{2-}$ are the products detected in less than 1.0 min.[60]

Mössbauer Spectrum of [Me_2Dabco][$Fe_2O(ttha)$]. Mössbauer spectroscopy is a useful technique for obtaining structural, oxidation-state, and spin-state information about iron complexes.[53,54] The Mössbauer spectrum of [Me_2Dabco][$Fe_2O(ttha)$]·$6H_2O$ is presented in Figure 8. The two experimental parameters obtained from the spectrum are presented in Table III along with data from other oxo-bridged systems and their related monomers. The isomer shift observed for $Fe_2O(ttha)^{2-}$ is identical with the isomer shift of $[Fe(hedta)]_2O^{2-}$ observed by Schugar, Rossman, Barraclough, and Gray[10] (0.63 mm/s). The data establish the high-spin $^6A_1$ ground state. The quadrupole splitting of $Fe_2O(ttha)^{2-}$ (1.56 mm/s) is close to the value observed for $[enH_2][Fe(hedta)]_2O$ (1.69 mm/s).

Conclusions

The mechanism of autoxidation of $Fe^{II}_2(ttha)^{2-}$ shows a step (k_1) that is associated with ring closure of the remaining Fe(II) site with the Fe(III)–O_2^- neighboring site. The intermediate may also be described as having $Fe^{IV}O_2^{2-}$ or $Fe^{II}(O_2)$ character. This evidence supports an open-chain structure for the $Fe^{II}_2(ttha)^{2-}$

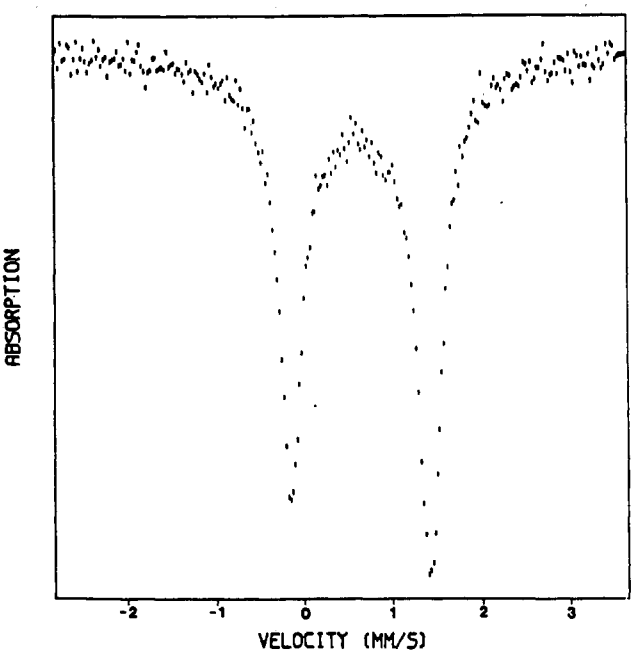

Figure 8. Mössbauer spectrum of $[Me_2Dabco][Fe_2O(ttha)]\cdot 6H_2O$.

Table III. Mössbauer Parameters of Selected Pairs of Monomers and Oxo-Bridged Dimers[a]

	isomer shift (δ)	quadrupole splitting (Δ)
$[Me_2Dabco][Fe_2O(ttha)]\cdot 6H_2O$[b]	0.63	1.56
$[enH_2][(Fe(hedta))_2O]\cdot 6H_2O$	0.63	1.69
$Fe(hedta)\cdot 1.5H_2O$	0.68	0.80
$Na_4[(Fe(edta))_2O]\cdot 12H_2O$	0.66	1.82
$Na[Fe(edta)]\cdot 3H_2O$	0.66	0.75
$[(Fe(terpy))_2O](NO_3)_4\cdot H_2O$	0.79	1.93
$Fe(terpy)Cl_3$	0.69	0.54
$Fe(Salen)_2O\cdot 2py$	0.71	0.92
$Fe(Salen)Cl\cdot xCH_3NO_2$	0.70	1.34

[a] All data are expressed in mm/s relative to a $Na_2Fe(CN)_5NO\cdot 2H_2O$ absorber: first complex, Fe_2Ottha^{2-}, from this work, all others from ref 10. [b] Full peak width at half-maximum is 0.32 mm/s.

complex, as was suggested previously from titration studies.[4] The UV–visible spectrum also shows no evidence for interaction of the two Fe(II) sites of $Fe^{II}_2(ttha)^{2-}$. An open-chain complex $Fe_2(ttha)(H_2O)_2$ has now been isolated for Fe(III). The initial monooxygenated species is assumed to be a bound superoxo intermediate in the $Fe_2(ttha)/O_2$ reaction on the basis of its oxidizing properties toward its own ligand structure in its coordination sphere and the kinetic evidence stated above. The second Fe(II) is tethered by the $ttha^{6-}$ polyamino carboxylate ligand at a close distance to the $Fe^{III}O_2^-$ site. The presence of a nearby reducing agent and the stability of the oxo-bridged Fe(III) binuclear product, due to spin exchange,[55] favors the net oxidation of $Fe^{II}_2(ttha)^{2-}$ to form $Fe_2O(ttha)^{2-}$. As no $HO^\bullet$ is detectable in abundance from the spin-trapping studies, the last rapid step in the reduction sequence must involve atom transfer from the peroxo intermediate to another $Fe^{II}_2(ttha)^{2-}$ reductant. A one-electron process involved in the rapid steps forming $Fe_2O(ttha)^{2-}$ would liberate a trappable $HO^\bullet$.

The difference in the reduced hemerythrin binding O_2 as a stable peroxide compared to the complete reduction of the O_2 to water with $Fe_2(ttha)^{2-}$ appears to be related to structural and concentration factors. The hemerythrin core structure retains the Fe(II) sites in neighboring proximity. Binding of O_2 yields a peroxo complex equivalent to the initial 2e reduction product of the $O_2/Fe^{II}_2(ttha)^{2-}$ reaction shown in Figure 6. However, the homogeneous solution peroxo species is not constrained from diffusion into the vicinity of other Fe(II) reducing centers. Rapid reduction of the coordinated peroxo complex by the available Fe(II) pool completes the net reduction to water of the original O_2 ligand; the stability of the oxo-bridged product favors net oxidation.[55] The large size and low effective concentration of the binuclear hemerythrin metalloprotein favor stopping the reduction scheme at the stage of the peroxo species. A hydrophobic region around the enzyme site would favor blocking the protonation step (k_2 in our scheme). The remaining earlier reaction steps are seen to be reversible, leading to oxygen loading and unloading according to the LeChatelier effect, depending on the O_2 pressure. The dependence on $[H_3O^+]$ shows an approach to saturation in scavenging of the $Fe^{III}O_2^{2-}Fe^{III}$ intermediate at the k_1 step even at pH 5.7. Therefore, the exclusion of H_3O^+ through hydrophobicity, or by pH control in the region of bound peroxo ligand by means of basic amino acid residues, could readily stabilize the bound peroxo complex. Indeed, the X-ray data on the hemerythrin protein show the O_2 binding site to be buried; binding of small molecules such as O_2, N_3^-, or NCS^- requires a long migration through a hydrophobic space.[56] No change in pH occurs upon oxygenation of the reduced enzyme.[57]

In this way the relatively hard donor ligand set of carboxylates and histidines can still yield a reversible O_2 carrier by favoring a hard Fe(III)–peroxo interaction as opposed to the soft Fe(II)–π-acceptor O_2 interaction for the heme-based O_2 carriers.

The Fe(III) oxidation product has been characterized as $Fe_2O(ttha)^{2-}$ on the combined evidence of pH titration data,[4] the spectrum very similar to that of the well-characterized $[Fe(hedta)]_2O^{2-}$ complex,[9-12] an Fe–O–Fe asymmetric stretch at 833 cm^{-1} for the Me_2Dabco^{2+} salt, and the close equivalency of the isomer shift and quadrupole splitting in the Mössbauer spectrum of $Me_2Dabco[Fe_2O(ttha)]$ with those of $[enH_2][(Fe(hedta))_2O]\cdot 6H_2O$.

The results of the spin-trapping experiments and the concurrence of the negative evidence in the kinetic studies as supplied by the presence of SOD and catalase scavengers show that the dominant reaction pathway for the $O_2/Fe_2(ttha)^{2-}$ reaction is the inner-sphere route to reduction of O_2 and its H_2O_2 intermediate. The absence of HODMPO$^\bullet$ adduct formed in this process shows that the rapid step that destroys the peroxo intermediate must be a very rapid *2e* reduction of the coordinated peroxide. If the process involved sequential one-electron reductions, a significant amount of $HO^\bullet$ should be released to solution for trapping. This is shown by the direct experimental observation of $HO^\bullet$ production in the $H_2O_2/Fe_2(ttha)^{2-}$ reaction (Figure 7A) where the initially separated Fe(II) centers execute the normal one-electron reduction of H_2O_2. This forms $HO^\bullet$, which escapes the solvent cage for DMPO trapping faster than the reduction of the initial $HO^\bullet$ product by the nearby second Fe(II) site within the same complex. The results are the same as those found for the $H_2O_2/Fe(edta)^{2-}$ reaction.[46,52] This fact provides added information that the $Fe_2(ttha)^{2-}$ complex exists in the open-chain configuration in solution.

Acknowledgment. We gratefully acknowledge the support of the National Science Foundation through NSF Grant CHE-8417751 and the donors of the Petroleum Research Fund, administered by the American Chemical Society. We thank Dr. R. Garrell for use of the Raman instrumentation.

Registry No. $Fe_2(ttha)^{2-}$, 101307-91-9; $[Me_2Dabco][Fe_2O(ttha)]$, 112506-07-7.

Supplementary Material Available: Figure 1SM, the Raman spectrum of the $Fe_2O(ttha)^{2-}$ ion in solution from 1400 to 1800 cm^{-1} (1 page). Ordering information is given on any current masthead page.